

# Network Topology in Water Nanoconfined between Phospholipid Membranes

Fausto Martelli,<sup>\*,†</sup> Jason Crain,<sup>†,‡</sup> and Giancarlo Franzese<sup>¶</sup>

<sup>†</sup>*IBM Research Europe, Hartree Centre, Daresbury, WA4 4AD, United Kingdom*

<sup>‡</sup>*Department of Biochemistry, University of Oxford, South Parks Road, Oxford, OX1 3QU,  
United Kingdom*

<sup>¶</sup>*Secció de Física Estadística i Interdisciplinària–Departament de Física de la Matèria  
Condensada, Universitat de Barcelona, & Institut de Nanociència i Nanotecnologia  
(IN2UB), Universitat de Barcelona, C. Martí i Franquès 1, 08028 Barcelona, Spain*

E-mail: fausto.martelli@ibm.com

## Abstract

Water provides the driving force for the assembly and stability of many cellular components. Despite its impact on biological functions, a nanoscale understanding of the relationship between its structure and dynamics under soft confinement has remained elusive. As expected, water in contact with biological membranes recovers its bulk density and dynamics at  $\sim 1$  nm from phospholipid headgroups but surprisingly enhances its intermediate-range order (IRO) over a distance, at least, twice as large. Here, we explore how the IRO is related to the water's hydrogen bond network (HBN) and its coordination defects. We characterize the increased IRO by an alteration of the HBN up to more than eight coordination shells of hydration water. The HBN analysis emphasizes the existence of a bound-unbound water interface at  $\sim 0.8$  nm from the membrane. The unbound water has a distribution of defects intermediate between bound and bulk water, but with density and dynamics similar to bulk, while bound

water has reduced thermal energy and much more HBN defects than low-temperature water. This observation could be fundamental for developing nanoscale models of biological interactions and for understanding how alteration of the water structure and topology, for example, due to changes in extracellular ions concentration, could affect diseases and signaling. More generally, it gives us a different perspective to study nanoconfined water.

## Keywords

water confined, phospholipid membrane, hydrogen bond, hydrogen bond network, coordination defects, order parameter

It has been long recognized that the structure and function of biological membranes are largely determined by the properties of hydration water, *i.e.*, of the water in contact with the membrane.<sup>1</sup> Indeed, the presence of water strongly influences membrane stability, fluidity, and phase behavior, thereby affecting membrane function and properties. Also, hydration water mediates the interactions of biological membranes with other biomolecules and with ions.<sup>2,3</sup>

Biological membranes are composed of a large number of components, including proteins, cholesterol, glycolipids, and ion channels, among others, but their framework is provided by phospholipid molecules that self-assemble into bilayers driven by the hydrophobic effect.<sup>1-16</sup> To decrease the interfacial free-energy, polar head groups form contacts with water, while the apolar hydrocarbon tails minimize exposure to water forming extended bilayers. Water is abundant in the interfacial region of bilayers (lipid headgroups), establishing strong hydrogen bonds (HBs) with the membrane. As a result of these strong interactions, the orientational and translational dynamics of interfacial water is markedly slowed down.<sup>6-9,14-16</sup> Such slowing down has been observed also in water in contact with proteins and sugars.<sup>17-21</sup>

Recently we found an increase in the structural order at the intermediate range when the dynamics of water confined by phospholipid membranes slows down. This intermediate

range order (IRO) propagates as far as (at least)  $\sim 2.4$  nm from the membrane surface,<sup>22</sup> a larger distance than previously calculated using other observables such as density and dynamical properties. We recovered water’s bulk density and dynamical properties at a distance of  $\sim 1.2$  nm from the membrane surface.<sup>22,23</sup> Nonetheless, water is a complex network-forming material, with a directional HBs network (HBN), the topology of which is correlated to anomalous behavior, as we showed recently.<sup>24</sup> Therefore, understanding how the HBN of water is affected by the interactions with the membrane is of primary importance in understanding biological properties at the molecular scale also in conditions in which a biological membrane interacts with alien components such as, *e.g.*, viruses.

In this article, we investigate the properties of water confined by phospholipid membranes. Specifically, we measure the extent to which phospholipid membranes affect the structural properties of water as well as its HBN. As a typical model membrane, we use 1,2-Dimyristoyl-*sn*-glycero-3-phosphocholine (DMPC) lipids. The DMPC is a phospholipid with a choline headgroup and a tailgroup formed of two myristoyl chains(see fig. 1). Choline-based phospholipids are ubiquitous in cell membranes and commonly used in drug-targeting liposomes.<sup>25</sup> In this investigation, we probe the structural properties of water by inspecting

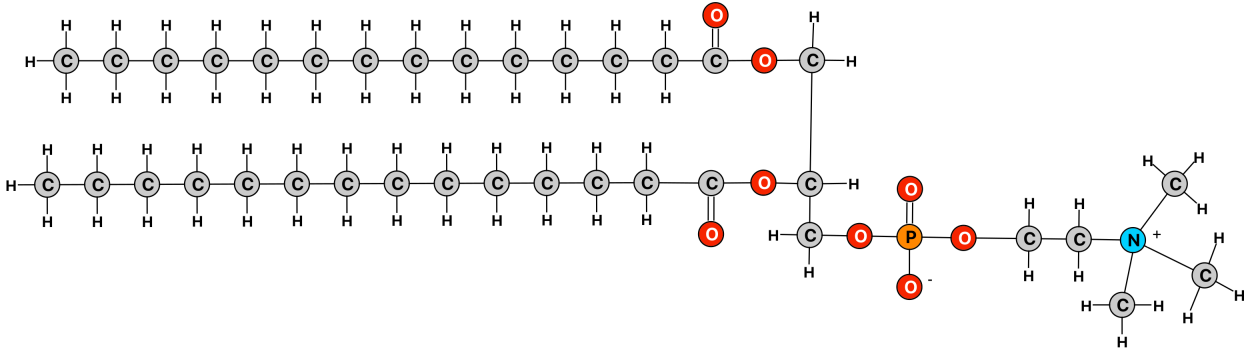


Figure 1: Chemical structure of the DMPC phospholipid.

the IRO using a sensitive local metric, recently introduced by Martelli *et al.*<sup>26</sup> and already applied in a wide variety of studies.<sup>22-24,26-28</sup> Next, we examine the topology and the quality

of the HBN and explore correlations of these observables with the behaviour of the structural order. We probe the topology of the HBN *via* ring statistics, a tool widely adopted in network-forming materials as a measure of closed loops present in the network. Ring statistics have been previously employed in water to characterize its different phases,<sup>26,27,29–31</sup> as well as to investigate the origin of water anomalies.<sup>24,32–35</sup>

## Results

We inspect the IRO by computing the score function (Eq. 2), which provides a nonlinear measure of the deviation in atomic or molecular arrangements from those of a reference structure that, usually, corresponds to the medium’s ground state at  $T = 0$  K. Therefore, we here compute  $S$  using, as a reference, the position of the oxygen in the second coordination shell in cubic ice, *i.e.*, a cuboctahedron ( $\bar{C}$ ) that belongs to the class of Archimedean solids enriched with edge transitivity<sup>36</sup> (inset in fig. 2). Similar results hold if we use, as a reference, the position of the oxygen in the second coordination shell in hexagonal ice.

At fixed  $T = 303$  K and  $P = 1$  atm, we compare the distributions of  $S_{\bar{C}}$  for bulk water and confined water at a distance of  $1.6 \text{ nm} \leq z \leq 2.4 \text{ nm}$  (bin centered at 2.0 nm) and  $2.4 \text{ nm} \leq z \leq 3.2 \text{ nm}$  (bin centered at 2.8 nm) from the membrane (fig. 2 a). We emphasize that the bin width of 0.8 nm adopted in this work ensures that water molecules centered in the middle of the bin have a second shell of neighbours falling inside the same bin.

The distribution at 2.0 nm does not match that of bulk water. In particular, we find that water 2.0 nm away from the membrane is more structured than bulk water, with a  $\sim 8\%$  increase of the  $S_{\bar{C}}$  with maximum probability, and a higher population in the large- $S_{\bar{C}}$  tail of the probability distribution  $P(S_{\bar{C}})$  (fig. 2 b).

On the other hand, the  $P(S_{\bar{C}})$  for water at 2.8 nm from the membrane overlaps with that of bulk water, within our resolution, showing that the value of the local order metric (LOM) of water between 2.4 nm and 3.2 nm is not affected by the membrane. Hence, our

result implies that the effect of the membrane on the structural properties of water should extend as far as 1.6 nm plus the second coordination shell distance ( $\sim 0.45$  nm<sup>37</sup>), and at about 2.4 nm minus 0.45 nm, *i.e.*, up to  $(2.0 \pm 0.05)$  nm, approximately (fig. 2 b).

Since the properties of water emanate from the underlying network of HBs,<sup>24</sup> a natural question follows: Is there a connection between i) the observed perturbations on the IRO of confined water, ii) the underlying HBN, and iii) its quality in terms of broken and intact HBs? We will address this question in the following discussion.

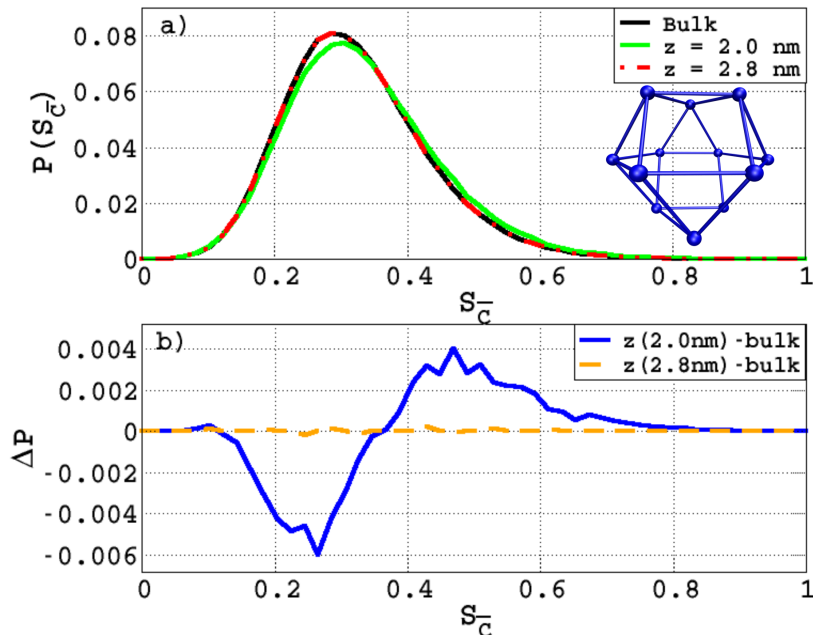


Figure 2: Panel a): Probability distributions of score function  $S_{\bar{C}}$  computed using the reference in the inset: the black line is for bulk water, the green line is for water in the bin centered at  $z = 2.0$  nm, the red dashed line is for water in the bin centered at  $z = 2.8$  nm. Inset: Reference made of the oxygen positions (blue spheres) of the second coordination shell in cubic ice. Blue sticks are a guide to the eyes to emphasize the geometrical structure. Panel b): Difference  $\Delta P$  between  $P(S_{\bar{C}})$  for bulk water and for the bin at  $z = 2.0$  nm (blue, continuous line), and between bulk water and the bin at  $z = 2.8$  nm (orange, dashed line).

We probe the HBN of water using the ring statistics, and we inspect the quality of the network quantifying and characterizing coordination defects. We compare the probability  $P(n)$  of having an  $n$ -member ring,  $n \in [3, 12]$ , for the four bins that discretize the simulation box, and for bulk water at the same thermodynamic conditions,  $T = 303$  K and  $P = 1$  atm

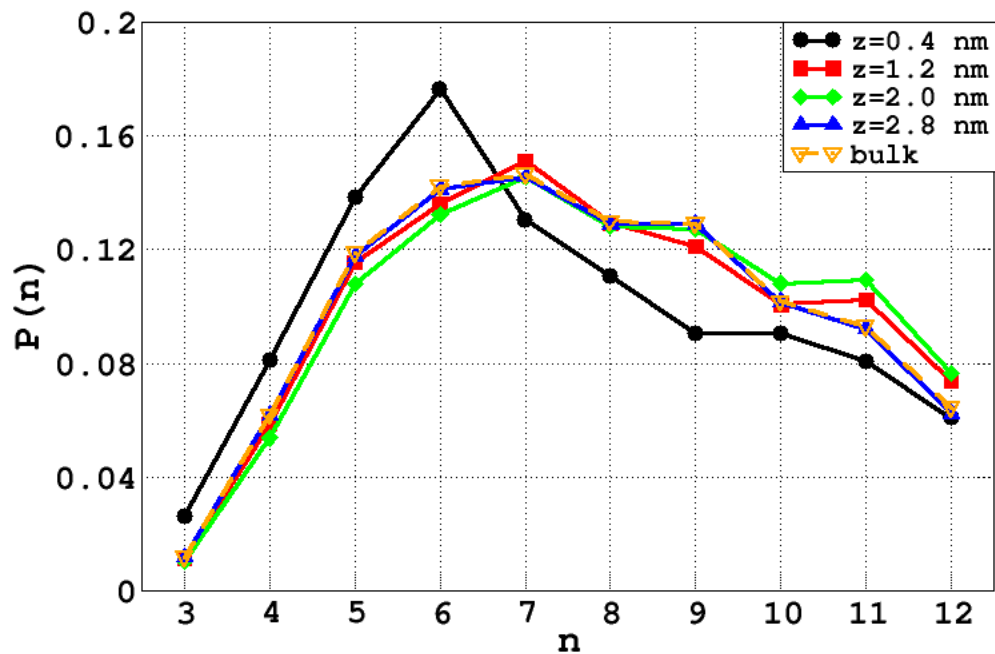


Figure 3: Probability of the HB  $n$ -member rings,  $P(n)$ , computed from structures in bulk water (open orange triangles), and in water in bins centered at different distances from the membrane surfaces: 0.4 nm (black dots), 1.2 nm (red squares), 2.0 nm (green diamonds), and 2.8 nm (blue triangles). All  $P(n)$  are normalized to unity and, therefore, do not reflect the total number of rings of a given size.

(fig. 3).

For bulk water, as expected in diffusive media,  $P(n)$  is broad and accounts for very large rings. We find that for distances within the bin closer to the bilayer, *i.e.*, at a distance  $z \leq 0.8$  nm from the membrane,  $P(n)$  strongly deviates from the corresponding probability in bulk water. Namely, we observe a depletion in the number of larger rings and an increase, notably sharp in the case of  $n = 6$ , of shorter rings. We attribute the depletion of larger rings to the proximity of the membrane, which represents a reduction of dimensionality in the connectivity search pathways of water molecules. On the other hand, we remark that  $n = 6$  represents the typical connectivity in crystalline ice. Therefore, the increased number of hexagonal rings at  $z = 0.8$  nm indicates that, closer to the interface, the HBN seems to acquire a topology closer to that of an ordered crystalline network. However, as we will discuss later, this similarity is only apparent.

The increased number of short rings at  $z \leq 0.8$  nm from the membrane is in agreement with the dynamical slowing down,<sup>38</sup> and the increment in the IRO<sup>22</sup> reported for similar distances. Hence, 1) the diffusion and rotational slowing down,<sup>38</sup> 2) the increased value of  $S_{\bar{C}}$  (fig. 2), and 3) the increased fraction of hexagonal rings (fig. 3) for water at  $z \leq 0.8$  nm from the membrane, suggest a connection between dynamics and structure as measured by i) the positions of the oxygen atoms and, ii) the topology of the HBN.

Moving from  $z \leq 0.8$  nm to  $0.8 \text{ nm} < z \leq 2.4$  nm, we observe a marked change in the distribution of  $n$ -rings with a decrease for  $n \leq 6$  and an increase for  $n > 6$  (fig. 3). We attribute the larger probability for extended rings for  $z > 0.8$  nm to the increased dimensionality of the space available. In particular, the difference in the  $P(n)$  and in the  $S_{\bar{C}}$  (fig. 2), between bulk and water within the bin centered at  $z = 2.0$  nm from the membrane, further points toward a close correlation between structural properties at the level of the medium range, and the topology of the HBN.

The drastic change in the ring probability between the bin centered in  $z = 0.4$  nm and the bins at a larger distance, is consistent with the recent discovery of an interface between bound

and unbound hydration water at about 0.5 nm from the membrane.<sup>38</sup> In Ref.<sup>38</sup> Calero and Franzese identify the interface between i) the first hydration shell, partially made of water bound to the membrane, with a structural role and an extremely slow dynamics, and ii) the next shells with no water-lipids HBs and a dynamics ten time faster than bound water, but still one order of magnitude slower than bulk water. Therefore, ring probability can mark the structural difference between bound and unbound water.

Moving to a distance  $2.4 \text{ nm} < z \leq 3.2 \text{ nm}$  from the surface, the  $P(n)$  overlaps perfectly with the bulk case. Moreover, the  $P(S_{\bar{C}})$  computed within this bin (fig. 2) overlaps with the  $P(S_C)$  of bulk water. Therefore, we conclude that water recovers the structural (both IRO and HBN) properties of bulk water only if at a distance larger than 2.4 nm from the membrane. This value is twice the 1.2 nm at which water retrieves bulk density and dynamics.<sup>22,23</sup>

To get further insights into the network topology, we inspect its quality. When water is in the glass state, we can map its HBN to a nearly-hyperuniform network, *i.e.*, to a continuous random network characterized by a low fraction of coordination defects and a suppression of long-range density fluctuations.<sup>39</sup> Therefore, the number of broken HBs is a measure of the quality of the HBN. In particular, it quantifies how far the HBN is from the two extreme cases: a) the liquid and b) the continuous random network. Furthermore, coordination defects directly affect the fluidity of liquid water. Therefore, they can be related to water dynamics.<sup>40</sup>

We perform a decomposition of the HBs per water molecule into acceptor-(A) and donor-(D) types. We label as  $A_2D_2$  a water molecule with perfect coordination, *i.e.*, donating two bonds and accepting two bonds. We evaluate the quality of the HBN by computing the ratio of water molecules that have different coordination, *i.e.*, are not in the  $A_2D_2$  configuration. In particular, we focus our attention on the following coordination configurations:  $A_1D_1$ ,  $A_2D_1$ ,  $A_1D_2$ ,  $A_2D_2$  and  $A_3D_2$ . Other configurations do not contribute significantly.<sup>41</sup>

We compare the percentage of intact HBs for bulk and confined water, as a function of

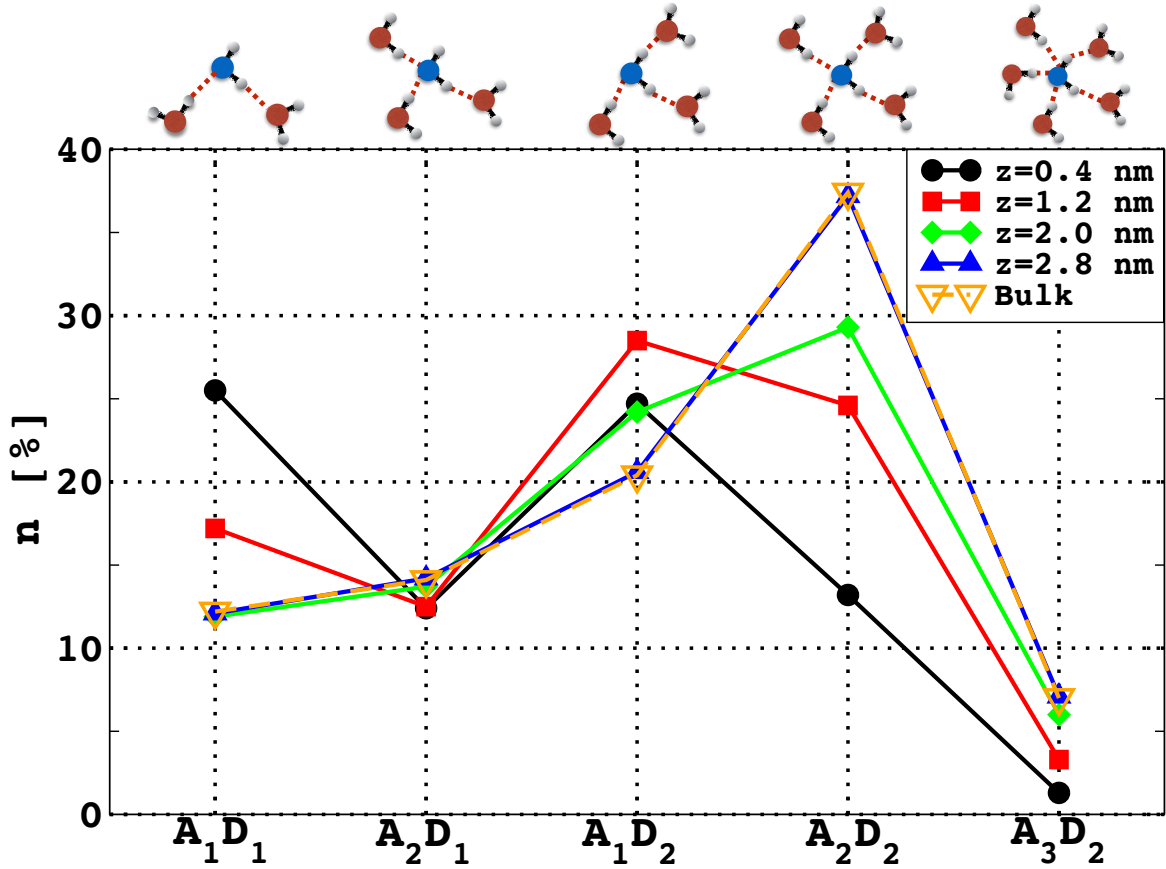


Figure 4: Percentage-wise decomposition of the intact HBs per water molecule into acceptor-(A) and donor-(D) for water in bins centered at different distances from the membrane and for bulk water. Sets are for bins at 0.4 nm (black dots), 1.2 nm (red squares), 2.0 nm (green diamonds), 2.8 nm (blue triangles) and bulk (orange open triangles). The  $x$ -axis labels  $A_x D_y$  indicate the number of acceptor ( $A_x$ ) and donor ( $D_y$ ) HBs, respectively, of the configurations schematically represented on the panel's top (with the oxygen of central water molecule in blue). For clarity we omit combinations with minor contributions, *e.g.*,  $A_3 D_1$ ,  $A_0 D_y$ ,  $A_x D_0$ , *etc.*

the distance from the membrane (fig. 4). We find that the HBN in bulk water is dominated by  $A_2D_2$  ( $\sim 37\%$ ) perfect coordinations. Water molecules involved in three HBs in the form of the defect  $A_1D_2$  comprise the next largest percentage ( $\sim 20\%$ ), followed by the  $A_2D_1$  and  $A_1D_1$  types and, finally, by the  $A_3D_2$ .

This result, based on TIP3P water, is in agreement with the trend in *ab initio* liquid water at ambient conditions examined with different functionals.<sup>41</sup> In particular, in *ab initio* liquid water, the frequency of  $A_1D_2$  is almost twice that of  $A_2D_1$  at all levels of theories.<sup>41</sup>

Close to the surface of the membrane, at  $z \leq 0.8$  nm, the network of HBs largely deviates from that of bulk water. The network is dominated by  $A_1D_1$  and  $A_1D_2$  defects ( $\sim 25\%$ ), followed by  $A_2D_1$  and  $A_2D_2$  configurations ( $\sim 15\%$ ), and a small percentage of higher coordination defects  $A_3D_2$  ( $\sim 3\%$ ). Such composition is very consistent with the results found for bound water at  $z \leq 0.5$  nm.<sup>38</sup> In particular, we find here the same percentage of defects with three water-water HBs (40%). Furthermore, we observe numbers, very close to those in Ref.<sup>38</sup>, for perfectly coordinated configurations ( $\sim 20\%$ ), and defects with two ( $\sim 30\%$ ) and five water-water HBs ( $\sim 1\%$ ).

However, close to the membrane, the decrease of perfectly coordinated water molecules seems to be inconsistent with the higher local order of water,<sup>22,23</sup> and also with the enhanced contribution of six-fold rings (fig. 3). This discrepancy is only apparent, for two reasons. First, both the IRO and the ring statistics are a measure of local order beyond short range, while the quality of the HBN is strictly a short-range measure. Second, our calculations include only water-water HBs and do not account for the (strong) HBs between water molecules and the phospholipid headgroups.<sup>38,42,43</sup> Instead,  $\sim 30\%$  of the water molecules in the first hydration shell are bound to the membrane with at least one HB.<sup>38</sup> This observation explains why the dynamical slowing down<sup>22</sup> of bound water can be interpreted as a local reduction of thermal noise that allows water molecules to organize in space in more ordered geometrical configurations.<sup>38</sup>

Moving away from the surface, at a distance of  $0.8 \text{ nm} < z \leq 2.4 \text{ nm}$ , the most apprecia-

ble effect on the quality of the HBN is a marked reduction of  $A_1D_1$  defects down to  $\sim 18\%$ , mostly accounting for the absence of HBs between water molecules and phospholipid head-groups,<sup>38</sup> and a corresponding drastic increase in the percentage of perfectly coordinated water molecules ( $A_2D_2$ ) up to  $\sim 25\%$ , confirming the analysis done for unbound water.<sup>38</sup>

At these distances bulk density and dynamical properties of water are recovered almost fully.<sup>22,38</sup> However, the quality (defects) of the HBN strongly deviates from that of bulk water, accounting for its different topology (ring probability, fig. 3) and its different structural properties.<sup>22</sup>

Upon increasing the distance from the membrane, we find a reduction of most of the coordination defects and a corresponding increase of perfectly coordinated water molecules, *i.e.*, an improvement in the quality of the HBN (fig. 4). Nevertheless, we recover the bulk-like composition only at a distance  $z > 2.4$  nm from the membrane, as in our analysis for both the IRO (fig. 2) and the topology of the HBN (fig. 3).

It is interesting to observe that the percentage of the defect type  $A_2D_1$  is mostly constant in all bins and, therefore, is independent of the distance from the membrane (fig. 4). We are currently working on rationalizing this intriguing evidence.

## Conclusions

The relation between water dynamics and structure is elusive in bulk<sup>44</sup> and even more under nanoconfinement,<sup>45</sup> especially when the confining surfaces are soft.<sup>46</sup> On the other hand, the relationships among the hydration structure and molecular fluidity at membrane/water interfaces are relevant in many biological processes.<sup>47</sup> Here, we study why water recovers its density and dynamics at  $\sim 1.2$  nm from a membrane<sup>22,38</sup> while has an intermediate range order (IRO)<sup>26</sup> higher than bulk up to a distance twice as large.<sup>22</sup> To understand this surprising result, we focus on the hydrogen bond network (HBN), analyzing its topology (ring statistics) and its quality (population of perfectly coordinated water molecules and

defects). We find that the increased IRO is characterized by an alteration of the HBN.

In particular, for bound water,<sup>38</sup> *i.e.*, water at short distances (here less than 0.8 nm) from the membrane, we show that the HBN topology and quality are very different from those of low-temperature bulk water. Although bound water has an HBN with a large fraction of hexagonal rings as in crystalline water, it has a much higher number of defects than low-temperature water. We find that  $A_1D_1$  and  $A_1D_2$  account together for 50% of all the defects due to water strong HBs with the membrane. These strong HBs locally reduce the water's thermal energy and slow down its dynamics.

We show that the HBN analysis is able to mark the existence of the bound-unbound water interface.<sup>38</sup> We find a sudden qualitative change in the ring statistics for hydration water at a distance  $z > 0.8$  nm from the membrane. Also the defects distribution clearly shows that water in the range  $0.8 \text{ nm} < z \leq 2.4 \text{ nm}$  is neither bound to the membrane, neither bulk. Indeed, it has much less  $A_1D_1$  defects than bound water, and much less perfectly-coordinated molecules than bulk. Nevertheless, at these distances, the structural differences between unbound and bulk water are disguised in water's density and dynamics.<sup>38</sup>

The difference in topology and defects smear out at distances larger than 2.4 nm. This distance corresponds to more than eight coordination shells of hydration water. Hence, our results support the evidence of long-range effects measured in terahertz and dielectric relaxation experiments.<sup>9,48-50</sup> We expect our conclusions to hold and eventually be emphasized by water potentials more realistic than TIP3P, which is quite poor in terms of structural properties beyond the short-range.

Our findings should be taken into account when interpreting experimental results and when developing membrane-water interaction potentials. They can help in better understanding water in biological processes at large, in particular those where hydration or structural changes play a role. Variations of ions concentration drastically change the water HBN<sup>51</sup> and its dynamics,<sup>52</sup> with an effect that is similar to an increase of pressure,<sup>53</sup> or a decrease of temperature for dehydration.<sup>38</sup> These variations in the extracellular matrix can

promote, for example, cardiac disease and arterial hardening in healthy men<sup>54</sup> or atherosclerosis and inflammatory signaling in endothelial cells.<sup>55</sup> Hence, our results entail further investigation about the relationship between this category of diseases with the water HBN rearrangements due to changes in hydration or ionic concentrations.

## Methods

### Simulation details

The systems considered here have the same geometry as in our previous simulations<sup>22</sup> but with a 15% increase in hydration, *i.e.*, they are composed of 128 DMPC lipids in a bilayer and 8100 water molecules, with periodic boundary conditions in such a way that water is confined between the two sides of two replicas of the same membrane. We perform molecular dynamics (MD) simulations on IBM POWER8 machines with NVIDIA Kepler K80 GPUs using the simulation package NAMD 2.9<sup>56</sup> at a temperature of  $T = 303$  K and an average pressure of  $p = 1$  atm. We set the simulation timestep to 2 fs. We describe the structure of phospholipids and their mutual interactions by the recently parameterized force field CHARMM36,<sup>57,58</sup> which is able to reproduce the area per lipid in excellent agreement with experimental data. The water model employed in our simulations, consistent with the parametrization of CHARMM36, is the modified TIP3P.<sup>59</sup> We cut off the Van der Waals interactions at 12 Å with a smooth switching function starting at 10 Å. We compute the long-ranged electrostatic forces with the particle-mesh Ewald method,<sup>60</sup> using a grid spacing of 1 Å. Our simulation box is anisotropic, with  $L_z > L_x$ , with  $L_x = L_y$ . This anisotropy ensures that there are no errors caused by the calculation of long-range electrostatics. During the  $NpT$  simulations we always keep this condition, with  $\sim 5\%$  fluctuations for the values of  $L_x$ ,  $L_y$ , and  $L_z$ . After energy minimization, we equilibrate the hydrated phospholipid bilayers for 10 ns followed by a production run of 2 ns in the  $NpT$  ensemble at  $p = 1$  atm. The energy profile is shown in fig. 5.

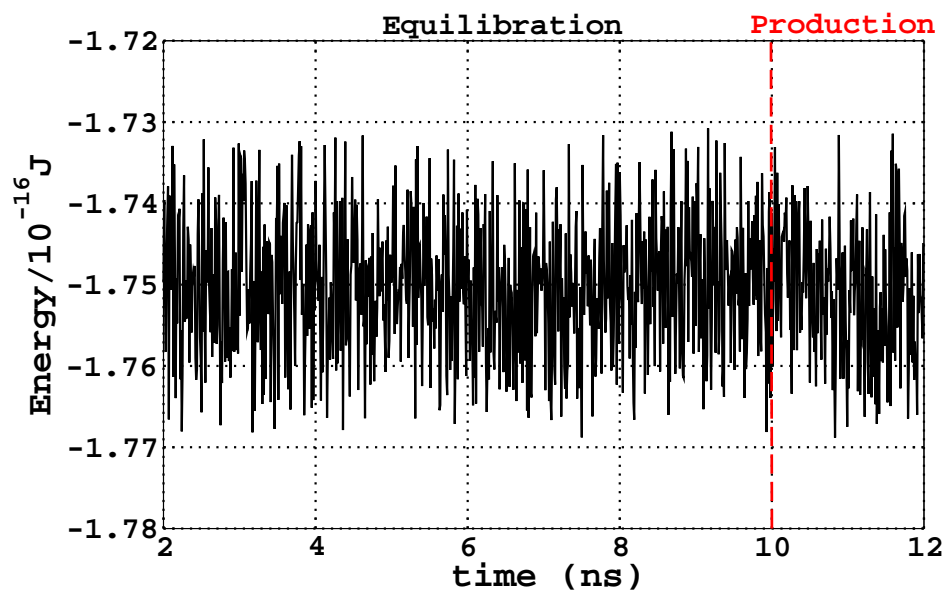


Figure 5: Energy profile for the system under consideration. The red dashed arrow defines the limit after which we start the production and data analysis.

In the simulations, we control the temperature with a Langevin thermostat<sup>61</sup> using a damping coefficient of  $0.1 \text{ ps}^{-1}$  and we control the pressure by a Nosé-Hoover Langevin barostat<sup>62</sup> with a piston oscillation time of 0.2 ps and a damping time of 0.1 ps. We also perform numerical simulations of bulk TIP3P water (4000 molecules) adopting the same protocol and at the same thermodynamic conditions. It is worthy to mention, at this point, that the isotropic  $NpT$  ensures that experimental observables such as, *e.g.*, the area per lipid and NMR order parameters, are properly reproduced.<sup>63-65</sup>

In order to investigate the IRO and the HBN, we divide the systems along the direction perpendicular to the phospholipid bilayer in equally spaced bins such that the thickness of each bin is 0.8 nm. This thickness is chosen in such a way that a molecule of water in the bin's center has, approximately, its second coordination shell included in the same bin at  $T = 303 \text{ K}$  and  $P = 1 \text{ atm}$ . For our hydration and bin's size, the two membranes are separated by eight bins, hence we can analyze four different distances between 0 and 3.2 nm. All the distances are measured taking as reference distance, for each side of the membrane, the position where the phospholipid density distribution, at thermodynamic equilibrium, has a maximum. We measure the observables of interest for each water molecule within each bin centered at a distance  $z$  from the center of the bilayer. It is worthy to mention that several more sophisticated ways of computing the distances from a rough membrane surface have been reported in the literature.<sup>38,66</sup> On the other hand, such methods show differences with respect to our approach when thinner bins are implemented and only in the proximity of the surface.

## The local order metric

We here briefly discuss the basic ideas behind the LOM we have used to probe the structural properties of water. Details can be found in Ref.<sup>26</sup>

The local environment of a water molecule  $j$  in a snapshot defines a local *pattern* formed by  $M$  neighboring sites. Here, we consider only the oxygen atoms' second neighbors of the

oxygen of the molecule  $j$ .

There are  $N$  local patterns, one for each atomic site  $j$  in the system. Indicating by  $\mathbf{P}_i^j (i = 1, M)$  the position vectors in the laboratory frame of the  $M$  neighbors of site  $j$ , their centroid is given by  $\mathbf{P}_c^j \equiv \frac{1}{M} \sum_{i=1}^M \mathbf{P}_i^j$ . In the following we refer the positions of the sites of the pattern to their centroid, *i.e.*  $\mathbf{P}_i^j - \mathbf{P}_c^j \rightarrow \mathbf{P}_i^j$ .

The local *reference* is a set of  $M$  sites, labeled by indices  $i (i = 1, M)$ , located at positions  $\mathbf{R}_i^j$  around the molecules  $j$  in ideal positions, typically as in a lattice of choice. The step of the reference lattice is fixed equal to equilibrium O–O distance,  $d$ , in the water coordination shell at the thermodynamic conditions of interest.

For each oxygen site  $j$  the centroid of the reference is set to coincide with the centroid of the pattern. The reference orientation is, instead, arbitrary, forming angles  $\theta, \phi, \psi$  with the pattern.

The LOM  $S(j)$  at site  $j$  is the maximum of the overlap function with respect to the orientation of the reference and the permutation of the pattern indices,

$$S(j) \equiv \max_{\theta, \phi, \psi; \mathcal{P}} \prod_{i=1}^M \exp \left( -\frac{|\mathbf{P}_{i_{\mathcal{P}}}^j - \mathbf{R}_i^j|^2}{2\sigma^2 M} \right). \quad (1)$$

Here  $i_{\mathcal{P}}$  are the permuted indices of the pattern sites corresponding to a permutation  $\mathcal{P}$ , and  $\sigma = d/4.4$  is a parameter that controls the spread of the Gaussian functions.

If  $L$  is the number of proper point symmetry operations of the reference, the overlap function (Eq. 1) has  $L$  equivalent maxima. Therefore, it is sufficient to compute  $S(j)$  for only a fraction  $1/L$  of the Euler angle domain  $\Omega$ , which we may call  $\Omega/L$ , the irreducible domain of the Euler angles. Inside  $\Omega/L$  we pick at random, with uniform probability, 15 orientations and we optimize them using a conjugate gradients procedure.

The LOM is an intrinsic property of the local environment at variance with the overlap function  $\mathcal{O}(j)$  that depends on the orientation of the reference and on the ordering of the sites in the pattern. The LOM satisfies the inequalities  $0 \lesssim S(j) \leq 1$ . The two limits

correspond, respectively, to a completely disordered local pattern ( $S(j) \rightarrow 0$ ) and to an ordered local pattern matching perfectly the reference ( $S(j) \rightarrow 1$ ), therefore grading each local environment on an increasing scale of local order from zero to one.

The order parameter *score function*  $S$  is the site-averaged LOM:

$$S \equiv \frac{1}{N} \sum_{j=1}^N S(j), \tag{2}$$

## Definition of rings

Several definitions of rings and counting schemes have been reported in the literature.<sup>67-73</sup> Recently, Formanek and Martelli have shown that different schemes allow us to access different information.<sup>74</sup>

Here, we construct rings as in fig. 6. We adopt the geometric definition of HB,<sup>75</sup> that is in qualitative agreement with other definitions over a wide range of thermodynamic conditions.<sup>76,77</sup> We start from a tagged water molecule and recursively traverse the HBN until we reached again the starting point, or we exceed the maximal ring size considered, 12 water molecules in our case. We consider only the primitive rings, *i.e.*, rings that can not be decomposed into smaller ones.<sup>67,71,78</sup> As shown in Ref.,<sup>74</sup> this definition provides a rich amount of information about the network.

## Acknowledgements

F.M. and J.C. acknowledge support from the STFC Hartree Centre’s Innovation Return on Research programme, funded by the Department for Business, Energy and Industrial Strategy. G.F. acknowledges support from the Spanish grant PGC2018-099277-B-C22 (MCIU/AEI/ERDF) and ICREA Foundation (ICREA Academia prize).

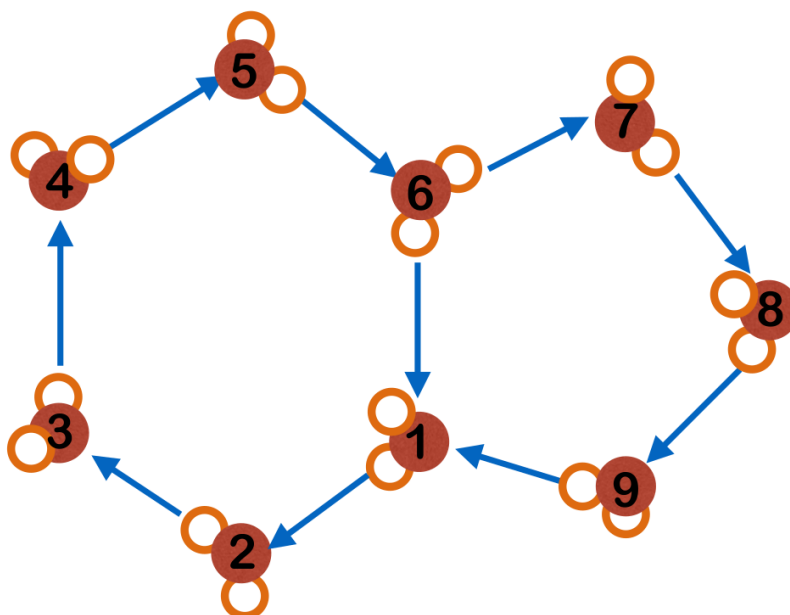


Figure 6: Schematic representation of the ring construction for a given HBN between water molecules. We start from water molecule labeled as 1 (O atoms are represented in red, H atoms in white). By following the directional HBs from H to O (blue arrows), we cross the HBN until we return to molecule 1 or we exceeds 12 steps and then take only those rings that cannot be decomposed in sub-rings. Here, we find a hexagonal ring from molecule 1 to 6 and and a pentagonal ring from 1 to 9.

## References

1. Berkowitz, M. L.; Bostick, D. L.; Pandit, S. Aqueous Solutions next to Phospholipid Membrane Surfaces: Insights from Simulations. *Chem. Rev.* **2006**, *106*, 1527–1539.
2. Yeagle, P. L., Ed. *The Structure of Biological Membranes*, 3rd ed.; CRC Press: New York, 2011.
3. Berkowitz, M. L., Ed. *Biomembrane Simulations: Computational Studies of Biological Membranes*, 1st ed.; Series in Computational Biophysics; CRC Press: New York, 2019.
4. Fitter, J.; Lechner, R. E.; Dencher, N. A. Interactions of Hydration Water and Biological Membranes Studied by Neutron Scattering. *J. Phys. Chem. B* **1999**, *103*, 8036–8050.
5. Trapp, M.; Gutberlet, T.; Juranyi, F.; Unruh, T.; Demé, B.; Tehei, M.; Peters, J. Hydration Dependent Studies of Highly Aligned Multilayer Lipid Membranes by Neutron Scattering. *J. Chem. Phys.* **2010**, *133*, 164505.
6. Wassall, S. R. Pulsed Field Gradient-Spin Echo NMR Studies of Water Diffusion in a Phospholipid Model Membrane. *Biophys. J.* **1996**, *71*, 2724–2732.
7. Volkov, V. V.; Palmer, D. J.; Righini, R. Distinct Water Species Confined at the Interface of a Phospholipid Membrane. *Phys. Rev. Lett.* **2007**, *99*, 078302.
8. Zhao, W.; Moilanen, D. E.; Fenn, E. E.; Fayer, M. D. Water at the Surfaces of Aligned Phospholipid Multibilayer Model Membranes Probed with Ultrafast Vibrational Spectroscopy. *J. Am. Chem. Soc.* **2008**, *130*, 13927–13937.
9. Tielrooij, K. J.; Paparo, D.; Piatkowski, L.; Bakker, H. J.; Bonn, M. Dielectric Relaxation Dynamics of Water in Model Membranes Probed by Terahertz Spectroscopy. *Biophys. J.* **2009**, *97*, 2848–2492.
10. Hua, W.; Verreault, D.; Allen, H. C. Solvation of Calcium–Phosphate Headgroup Complexes at the DPPC/Aqueous Interface. *ChemPhysChem* **2015**, *16*, 3910–3915.

11. Róg, T.; Murzyn, K.; Pasenkiewicz-Gierula, M. The Dynamics of Water at the Phospholipid Bilayer Surface: A Molecular Dynamics Simulation Study. *Chem. Phys. Lett.* **2002**, *352*, 323–327.
12. Bhide, S. Y.; Berkowitz, M. L. Structure and Dynamics of Water at the Interface with Phospholipid Bilayers. *J. Chem. Phys.* **2005**, *123*, 224702.
13. von Hansen, Y.; Gekle, S.; Netz, R. R. Anomalous Anisotropic Diffusion Dynamics of Hydration Water at Lipid Membranes. *Phys. Rev. Lett.* **2013**, *111*, 118103.
14. Zhang, Z.; Berkowitz, M. L. Orientational Dynamics of Water in Phospholipid Bilayers with Different Hydration Levels. *J. Phys. Chem. B* **2009**, *113*, 7676–7680.
15. Gruenbaum, S. M.; Skinner, J. L. Vibrational Spectroscopy of Water in Hydrated Lipid Multi-Bilayers. I. Infrared Spectra and Ultrafast Pump-Probe Observables. *J. Chem. Phys.* **2011**, *135*, 075101.
16. Borallo, C. C.; Stanley, E. H.; Franzese, G. Structural Interpretation of the Large Slowdown of Water Dynamics at Stacked Phospholipid Membranes for Decreasing Hydration Level: All-Atom Molecular Dynamics. *Materials* **2016**, *9*, 319.
17. Camisasca, G.; Iorio, A.; Marzio, M. D.; Gallo, P. Structure and Slow Dynamics of Protein Hydration Water. *J. Mol. Liq.* **2018**, *268*, 903–910.
18. Iorio, A.; Camisasca, G.; Rovere, M.; Gallo, P. Characterization of Hydration Water in Supercooled Water–Trehalose Solutions: The Role of the Hydrogen Bonds Network. *J. Chem. Phys.* **2019**, *51*, 044507.
19. Iorio, A.; Camisasca, G.; Gallo, P. Glassy Dynamics of Water at Interface with Biomolecules: A Mode Coupling Theory Test. *Sci. China Phys. Mech.* **2019**, *62*, 107011.
20. Iorio, A.; Camisasca, G.; Gallo, P. Slow Dynamics of Hydration Water and the Trehalose Dynamical Transition. *J. Mol. Liq.* **2019**, *282*, 617–625.

21. Iorio, A.; Minozzi, M.; Camisasca, G.; Rovere, M.; Gallo, P. Slow Dynamics of Supercooled Hydration Water in Contact with Lysozyme: Examining the Cage Effect at Different Length Scales. *Philos. Mag* **2020**, *0*, 1–14.
22. Martelli, F.; Ko, H.-Y.; Borallo, C. C.; Franzese, G. Structural Properties of Water Confined by Phospholipid Membranes. *Front. Phys.* **2018**, *13*, 136801.
23. Samatas, S.; Calero, C.; Martelli, F.; Franzese, G. In *Biomembrane Simulations Computational Studies of Biological Membranes*; Berkowitz, M., Ed.; CRC Press: New York, 2019; p 69.
24. Martelli, F. Unravelling the Contribution of Local Structures to the Anomalies of Water: The Synergistic Action of Several Factors. *J. Chem. Phys.* **2019**, *150*, 094506.
25. Hamley, W. *Introduction to Soft Matter*; John Wiley and Sons, West Sussex, England, 2007.
26. Martelli, F.; Ko, H.-Y.; Oğuz, E. C.; Car, R. Local-Order Metric for Condensed Phase Environments. *Phys. Rev. B* **2016**, *97*, 064105.
27. Martelli, F.; Giovambattista, N.; Torquato, S.; Car, R. Searching for Crystal-Ice Domains in Amorphous Ices. *Phys. Rev. Materials* **2018**, *2*, 075601.
28. Santra, B.; Ko, H.-Y.; Yeh, Y.-W.; Martelli, F.; Kaganovich, I.; Raitses, Y.; Car, R. Root-Growth of Boron Nitride Nanotubes: Experiments and *Ab Initio* Simulations. *Nanoscale* **2018**, *10*, 22223.
29. Martoňák, R.; Donadio, D.; Parrinello, M. Polyamorphism of Ice at Low Temperatures from Constant-Pressure Simulations. *Phys. Rev. Lett.* **2004**, *92*, 225702.
30. Martoňák, R.; Donadio, D.; Parrinello, M. Evolution of the Structure of Amorphous Ice: From Low-Density Amorphous through High-Density Amorphous to Very High-Density Amorphous Ice. *J. Chem. Phys.* **2005**, *122*, 134501.

31. Camisasca, G.; Schlesinger, D.; Zhovtobriukh, I.; Pitsevich, G.; Pettersson, L. G. M. A Proposal for the Structure of High- and Low-Density Fluctuations in Liquid Water. *J. Chem. Phys.* **2019**, *151*, 034508.
32. Russo, J.; Tanaka, H. Understanding Water's Anomalies with Locally Favoured Structures. *Nat. Commun.* **2014**, *5*, 3556.
33. Palmer, J. C.; Martelli, F.; Liu, Y.; Car, R.; Panagiotopoulos, A. Z.; Debenedetti, P. G. Metastable Liquid-Liquid Transition in a Molecular Model of Water. *Nature* **2014**, *510*, 385–388.
34. Santra, B.; DiStasio Jr., R. A.; Martelli, F.; Car, R. Local Structure Analysis in *AbInitio* Liquid Water. *Mol. Phys.* **2015**, *113*, 2829–2841.
35. Ansari, N.; Ansari, N.; Onat, B.; Sosso, G. C.; Hassanali, A. Insights into the Emerging Networks of Voids in Simulated Supercooled Water. *J. Phys. Chem. B* **2020**, *124*, 2180–2190.
36. Read, R. C.; Wilson, J. R. *An Atlas of Graphs*; Oxford University Press: Oxford, 2016.
37. Mark, P.; Nilsson, L. Structure and Dynamics of the TIP3P, SPC, and SPC/E Water Models at 298 K. *J. Phys. Chem. A* **2001**, *105*, 9954–9960.
38. Calero, C.; Franzese, G. Membranes with Different Hydration Levels: The Interface between Bound and Unbound Hydration Water. *J. Mol. Liq.* **2019**, *273*, 488–496.
39. Martelli, F.; Torquato, S.; Giovambattista, N.; Car, R. Large-Scale Structure and Hyperuniformity of Amorphous Ices. *Phys. Rev. Lett.* **2017**, *119*, 136002.
40. de los Santos, F.; Franzese, G. Relations between the Diffusion Anomaly and Cooperative Rearranging Regions in a Hydrophobically Nanoconfined Water Monolayer. *Phys. Rev. E* **2012**, *85*, 010602–.

41. DiStasio Jr., R. A.; Santra, B.; Li, Z.; Wu, X.; Car, R. The Individual and Collective Effects of Exact Exchange and Dispersion Interactions on the *Ab Initio* Structure of Liquid Water. *J. Chem. Phys.* **2014**, *141*, 084502.
42. Binder, H. The Molecular Architecture of Lipid Membranes: New Insights from Hydration–Huning Infrared Linear Dichroism Spectroscopy. *Appl. Spectrosc. Rev.* **2003**, *30*, 15–69.
43. Chen, X.; Hua, W.; Huang, Z.; Allen, H. C. Interfacial Water Structure Associated with Phospholipid Membranes Studied by Phase–Sensitive Vibrational Sum Frequency Generation Spectroscopy. *J. Am. Chem. Soc.* **2010**, *132*, 1336–11342.
44. Verde, A. R.; Montes de Oca, J. M.; Accordino, S. R.; Alarcón, L. M.; Appignanesi, G. A. Comparing the Performance of Two Structural Indicators for Different Water Models while Seeking for Connections between Structure and Dynamics in the Glassy Regime. *J. Chem. Phys.* **2019**, *150*, 244504.
45. Joseph, S.; Aluru, N. R. Why Are Carbon Nanotubes Fast Transporters of Water? *Nano Letters* **2008**, *8*, 452–458.
46. Ruiz Pestana, L.; Felberg, L. E.; Head-Gordon, T. Coexistence of Multilayered Phases of Confined Water: The Importance of Flexible Confining Surfaces. *ACS Nano* **2018**, *12*, 448–454.
47. Asakawa, H.; Yoshioka, S.; Nishimura, K.-i.; Fukuma, T. Spatial Distribution of Lipid Headgroups and Water Molecules at Membrane/Water Interfaces Visualized by Three-Dimensional Scanning Force Microscopy. *ACS Nano* **2012**, *6*, 9013–9020.
48. Ebbinghaus, S.; Kim, S. J.; Heyden, M.; Yu, X.; Heugen, U.; Gruebele, M.; Leitner, D. M.; Havenith, M. An Extended Dynamical Hydration Shell around Proteins. *Proc. Natl. Ac. Sci. USA* **2007**, *104*, 20749–20752.

49. Zhang, C.; Gygi, F.; Galli, G. Strongly Anisotropic Dielectric Relaxation of Water at the Nanoscale. *J. Phys. Chem. Lett.* **2013**, *4*, 2477–2481.
50. Hishida, M.; Tanaka, K. Long-Range Hydration Effect of Lipid Membrane Studied by Terahertz Time-Domain Spectroscopy. *Phys. Rev. Lett.* **2013**, *106*, 158102.
51. Mancinelli, R.; Botti, A.; Bruni, F.; Ricci, M. A.; Soper, A. K. Perturbation of Water Structure Due to Monovalent Ions in Solution. *Phys. Chem. Chem. Phys.* **2007**, *9*, 2959–2967.
52. Fayer, M. D.; Moilanen, D. E.; Wong, D.; Rosenfeld, D. E.; Fenn, E. E.; Park, S. Water Dynamics in Salt Solutions Studied with Ultrafast Two-Dimensional Infrared (2D IR) Vibrational Echo Spectroscopy. *Acc. Chem. Res.* **2009**, *42*, 1210–9.
53. Gallo, P.; Corradini, D.; Rovere, M. Do Ions Affect the Structure of Water? The Case of Potassium Halides. *J. Mol. Liq.* **2014**, *189*, 52–56.
54. Arnaoutis, G.; Kavouras, S. A.; Stratakis, N.; Likka, M.; Mitrakou, A.; Papamichael, C.; Sidossis, L. S.; Stamatelopoulos, K. The Effect of Hypohydration on Endothelial Function in Young Healthy Adults. *Eur. J. Nutr.* **2017**, *56*, 1211–1217.
55. Dmitrieva, N. I.; Burg, M. B. Elevated Sodium and Dehydration Stimulate Inflammatory Signaling in Endothelial Cells and Promote Atherosclerosis. *PLOS ONE* **2015**, *10*, 1–22.
56. Phillips, J. C.; Braun, R.; Wang, W.; Gumbart, J.; Tajkhorshid, E.; Villa, E.; Chipot, C.; Skeel, R. D.; Kalé, L.; Schulten, K. Scalable Molecular Dynamics with NAMD. *J. Comput. Chem.* **2005**, *26*, 1781–1802.
57. Klauda, J. B.; Venable, R. M.; Freites, J. A.; O’Connor, J. W.; Tobias, D. J.; Mondragon-Ramirez, C.; Vorobyov, I.; MacKerell, A. D.; Pastor, R. W. Update of the CHARMM All-Atom Additive Force Field for Lipids: Validation on Six Lipid Types. *J. Phys. Chem. B* **2010**, *114*, 7830–7843.

58. Lim, J. B.; Rogaski, B.; Klauda, J. B. Update of the Cholesterol Force Field Parameters in CHARMM. *J. Phys. Chem. B* **2012**, *116*, 203–210.
59. Jorgensen, W. L.; Chandrasekhar, J.; Madura, J. D. Comparison of Simple Potential Functions for Simulating Liquid Water. *J. Chem. Phys.* **1983**, *79*, 926.
60. Essmann, U.; Perera, L.; Berkowitz, M. L. A Smooth Particle Mesh Ewald Method. *J. Chem. Phys.* **1995**, *103*, 8577.
61. Berendsen, H. J. C.; Postma, J. P. M.; van Gunsteren, W. F.; DiNola, A.; Haak, J. R. Molecular Dynamics with Coupling to an External Bath. *J. Phys. Chem.* **1984**, *81*, 3684.
62. Feller, S. E.; Zhang, Y.; Pastor, R. W.; Brooks, B. R. Constant Pressure Molecular Dynamics Simulation: The Langevin Piston Method. *J. Phys. Chem.* **1995**, *103*, 4613.
63. Taylor, J.; Whiteford, N. E.; Bradley, G.; Watson, G. W. Validation of All-Atom Phosphatidylcholine Lipid Force Fields in the Tensionless NPT Ensemble. *Biochim. Biophys. Acta* **2009**, *1788*, 638–649.
64. Davis, J. E.; Rahaman, O.; Patel, S. Molecular Dynamics Simulations of a DMPC Bilayer Using Nonadditive Interaction Models. *Biophys. J.*, **2009**, *96*, 285–402.
65. Gapsys, V.; de Groot, B. L.; Briones, R. Computational Analysis of Local Membrane Properties. *J. Comput. Aided Mol. Des.* **2013**, *27*, 845–858.
66. Pandit, S. A.; Bostick, D.; Berkowitz, M. L. An Algorithm to Describe Molecular Scale Rugged Surfaces and its Application to the Study of a Water/Lipid Bilayer interface. *J. Chem. Phys.* **2003**, *119*, 2199–2205.
67. King, S. V. Ring Configurations in a Random Network Model of Vitreous Silica. *Nature* **1967**, *213*, 1112–1113.
68. Rahman, A.; Stillinger, F. H. Hydrogen-Bond Patterns in Liquid Water. *J. Am. Chem. Soc.* **1973**, *95*, 7943–7948.

69. Guttman, L. Ring Structure of the Crystalline and Amorphous Forms of Silicon Dioxide. *J. Non-Cryst. Solids* **1990**, *116*, 145–147.
70. Franzblau, D. S. Computation of Ring Statistics for Network Models of Solids. *Phys. Rev. B* **1991**, *44*, 4925.
71. Wooten, F. Structure, Odd Lines and Topological Entropy of Disorder of Amorphous Silicon. *Acta Cryst. A* **2002**, *58*, 346–351.
72. Yuan, X.; Cormack, A. N. Efficient Algorithm for Primitive Ring Statistics in Topological Networks. *Comp. Mater. Sci.* **2002**, *24*, 343–360.
73. Roux, S. L.; Jund, P. Ring Statistics Analysis of topological Networks: New Approach and Application to Amorphous GeS<sub>2</sub> and SiO<sub>2</sub> Systems. *Comp. Mater. Sci.* **2010**, *49*, 70–83.
74. Formanek, M.; Martelli, F. Probing the Network Topology in Network-Forming Materials: the Case of Water. *AIP Adv.* **2020**, *10*, 055205.
75. Luzar, A.; Chandler, D. Hydrogen-Bond Kinetics in Liquid Water. *Nature* **1996**, *379*, 55–57.
76. Prada-Gracia, D.; Shevchuk, R.; Rao, F. The Quest for Self-Consistency in Hydrogen Bond Definitions. *J. Chem. Phys.* **2013**, *139*, 084501.
77. Shi, R.; Russo, J.; Tanaka, H. Common Microscopic Structural Origin for Water's Thermodynamic and Dynamic Anomalies. *J. Chem. Phys.* **2018**, *149*, 224502.
78. Goetzke, K.; Klein, H.-J. Properties and Efficient Algorithmic Determination of Different Classes of Rings in Finite and Infinite Polyhedral Networks. *J. Non-Cryst. Solids* **1991**, *127*, 215–220.